Terahertz quantum cascade lasers operating up to ~ 200 K with optimized oscillator strength and improved injection tunneling

S. Fathololoumi,[1,3,*] E. Dupont,[1] C.W.I. Chan,[2] Z.R. Wasilewski,[1] S.R. Laframboise,[1] D. Ban,[3] A. Mátyás,[4] C. Jirauschek,[4] Q. Hu,[2] and H. C. Liu[1,5]

[1] *Institute for Microstructural Sciences, National Research Council, 1200 Montreal Rd, Ottawa, ON, K1A0R6, Canada*
[2] *Department of Electrical Engineering and Computer Science, Research Laboratory of Electronics, Massachusetts Institute of Technology, Cambridge, MA 02139, USA*
[3] *Department of Electrical and Computer Engineering, Waterloo Institute for Nanotechnology, University of Waterloo, 200 University Ave W., Waterloo, ON, N2L3G1, Canada*
[4] *Institute for Nanoelectronics, Technische Universität München, D-80333 München, Germany*
[5] *Currently with Key Laboratory of Artificial Structures and Quantum Control, Department of Physics, Shanghai Jiao Tong University, Shanghai 200240, China*

[*] *sfatholo@uwaterloo.ca*

Abstract: A new temperature performance record of 199.5 K for terahertz quantum cascade lasers is achieved by optimizing the lasing transition oscillator strength of the resonant phonon based three-well design. The optimum oscillator strength of 0.58 was found to be larger than that of the previous record (0.41) by Kumar et *al*. [Appl. Phys. Lett. 94, 131105 (2009)]. The choice of tunneling barrier thicknesses was determined with a simplified density matrix model, which converged towards higher tunneling coupling strengths than previously explored and nearly perfect alignment of the states across the injection and extraction barriers at the design electric field. At 8 K, the device showed a threshold current density of 1 kA/cm^2, with a peak output power of $\sim$ 38 mW, and lasing frequency blue-shifting from 2.6 THz to 2.85 THz with increasing bias. The wavelength blue-shifted to 3.22 THz closer to the maximum operating temperature of 199.5 K, which corresponds to $\sim 1.28h\omega/\kappa_B$. The voltage dependence of laser frequency is related to the Stark effect of two intersubband transitions and is compared with the simulated gain spectra obtained by a Monte Carlo approach.

© 2012 Optical Society of America

OCIS codes: (140.5965) Semiconductor lasers, quantum cascade; (40.5960) Semiconductor lasers.

References and links

1. R. Kohler, A. Tredicucci, F. Beltram, H. E. Beere, E. H. Linfield, A. G. Davies, D. Ritchie, R. C. Iotti, and F. Rossi, "Terahertz semiconductor-heterostructure laser," Nature **417,** 156–159 (2002).
2. B. S. Williams, S. Kumar, Q. Hu, and J. L. Reno, "Operation of terahertz quantum-cascade lasers at 164 K in pulsed mode and at 117 K in continuous-wave mode," Opt. Express **13,** 3331–3339 (2005).
3. H. Luo, S. R. Laframboise, Z. R. Wasilewski, and H. C. Liu, "Terahertz quantum cascade lasers based on a three-well active module," Appl. Phys. Lett. **90,** 041112 (2007).

#157687 - $15.00 USD Received 21 Nov 2011; revised 17 Jan 2012; accepted 18 Jan 2012; published 1 Feb 2012

4. M. A. Belkin, J. A. Fan, S. Hormoz, F. Capasso, S. P. Khanna, M. Lachab, A. G. Davies, and E. H. Linfield, "Terahertz quantum cascade lasers with copper metal-metal waveguides operating up to 178 K," Opt. Express **16,** 3242–3248 (2008).
5. S. Kumar, Q. Hu, and J. L. Reno, "186 K operation of terahertz quantum cascade lasers based on a diagonal design," Appl. Phys. Lett. **94,** 131105 (2009).
6. S. Kumar, C. W. I. Chan, Q. Hu, and J. L. Reno, "A 1.8-THz quantum cascade laser operating significantly above the temperature of $h\omega/\kappa_B$," Nat. Phys. **7,** 166–171 (2011).
7. R. W. Adams, K. Vijayraghavan, Q. J. Wang, J. Fan, F. Capasso, S. P. Khanna, A. G. Davies, E. H. Linfield, and M. A. Belkin, "GaAs/$Al_{0.15}Ga_{0.85}$As terahertz quantum cascade lasers with double-phonon resonant depopulation operating up to 172 K," Appl. Phys. Lett. **97,** 131111 (2010).
8. S. Kumar, C. W. I. Chan, Q. Hu, and J. L. Reno, "Two-well terahertz quantum-cascade laser with direct intrawell-phonon depopulation," Appl. Phys. Lett. **95,** 141110 (2009).
9. G. Scalari, M. I. Amanti, C. Walther, R. Terazzi, M. Beck, and J. Faist, "Broadband THz lasing from a photon-phonon quantum cascade structure," Opt. Express **8,** 8043–8052 (2010).
10. A. Wacker, "Extraction-controlled quantum cascade lasers," Appl. Phys. Lett. **97,** 081105 (2010).
11. B. S. Williams, H. Callebaut, S. Kumar, Q. Hu, and J. L. Reno, "THz quantum cascade laser at $\lambda \approx 100\ \mu$m using metal waveguide for mode confinement," Appl. Phys. Lett. **83,** 2124–2126 (2003).
12. Q. Hu, B. S. Williams, S. Kumar, H. Callebaut, S. Kohen, and J. L. Reno, "Resonant-phonon-assisted THz quantum-cascade lasers with metal–metal waveguides," Semicond. Sci. Technol. **20,** S228–S236 (2005).
13. S. Fathololoumi, E. Dupont, S. G. Razavipour, S. R. Laframboise, G. Parent, Z. Wasilewski, H. C. Liu, and D. Ban, "On metal contacts of terahertz quantum-cascade lasers with a metal-metal waveguide," Semicond. Sci. Technol. **26,** 105021 (2011).
14. M. A. Belkin, Q. J. Wang, C. Pflügl, A. Belyanin, S. P. Khanna, A. G. Davies, E. H. Linfield, and F. Capasso, "High-temperature operation of terahertz quantum cascade laser sources," IEEE Sel. Top. Quantum Electron. **15,** 952–967 (2009).
15. R. Terrazi and J. Faist, "A density matrix model of transport and radiation in quantum cascade lasers," New J. Phys. **12,** 033045 (2010).
16. S. Kumar and Q. Hu, "Coherence of resonant-tunneling transport in terahertz quantum-cascade lasers," Phys. Rev. B **80,** 245316 (2009).
17. E. Dupont, S. Fathololoumi, and H. C. Liu, "Simplified density matrix model applied to three-well terahertz quantum cascade lsers," Phys. Rev. B **81,** 205311 (2010).
18. S. C. Lee and A. Wacker, "Nonequilibrium Greens function theory for transport and gain properties of quantum cascade structures," Phys. Rev. B **66,** 245314 (2002).
19. T. Kubis, C. Yeh, P. Vogl, A. Benz, G. Fasching, and C. Deutsch, "Theory of nonequilibrium quantum transport and energy dissipation in terahertz quantum cascade lasers," Phys. Rev. B **79,** 195323 (2009).
20. H. Callebaut, S. Kumar, B.S. Williams, Q. Hu, and J. L. Reno, "Analysis of transport properties of terahertz quantum cascade lasers," Appl. Phys. Lett. **83,** 207–209 (2003).
21. H. Callebaut and Q. Hu, "Importance of coherence for electron transport in terahertz quantum cascade lasers," J. Appl. Phys. **98,** 104505 (2005).
22. C. Jirauschek and P. Lugli, "Monte-Carlo-based spectral gain analysis for terahertz quantum cascade lasers," J. Appl. Phys. **105,** 123102 (2009).
23. A. Mátyás, M. A. Belkin, P. Lugli, and C. Jirauschek, "Temperature performance analysis of terahertz quantum cascade lasers: Vertical versus diagonal designs," Appl. Phys. Lett. **96,** 201110 (2010).
24. S. Fathololoumi, E. Dupont, S.R. Laframboise, Z. R. Wasilewski, D. Ban, and H. Liu , "Design of laser transition oscillator strength for THz quantum cascade lasers," Presented at Conference on Lasers and Electro-Optics, Baltimore, MD (2011).
25. H. Luo, S. R. Laframboise, Z. R. Wasilewski, and H. C. Liu, "Effects of injector barrier on performance of terahertz quantum-cascade lasers," IEEE Electron. Lett. **43,** 633–635 (2007).
26. H. Luo, S. R. Laframboise, Z. R. Wasilewski, H. C. Liu, and J. C. Cao, "Effects of extraction barrier width on performance of terahertz quantum-cascade lasers," IEEE Electron. Lett. **44,** 630–631 (2008).
27. For the density matrix calculations, the electron temperature was chosen 90 K higher than lattice. Pure dephasing time constants of tunneling $\tau^* = 0.35$ ps, and of optical intersubband transition $\tau^*_{\rm ul} = 1.1$ ps were used. Intrawell intersubband scatterings by LO phonon, e-impurities and interface roughness were considered. The momentum dependance of scattering is averaged over the assumed Maxwell-Boltzmann distribution of carriers in the subbands.
28. S. Fathololoumi, E. Dupont, Z. R. Wasilewski, S. R. Laframboise, D. Ban, and H. C. Liu, "Effect of intermediate resonance on the performance of resonant phonon based terahertz quantum cascade laser," Presented at 11th International Conference on Intersubband Transitions in Quantum Wells, Badesi, Italy (2011).
29. S. Fathololoumi, D. Ban, H. Luo, E. Dupont, S. R. Laframboise, A. Boucherif, and H. C. Liu, "Thermal behavior investigation of terahertz quantum-cascade lasers," IEEE J. Quantum Electron. **44,** 1139–1144 (2008).
30. S. Fathololoumi, E. Dupont, D. Ban, M. Graf, S. R. Laframboise, Z. Wasilewski, and H. C. Liu, "Time-resolved thermal quenching of THz quantum cascade lasers," IEEE J. Quantum Electron **46,** 396–404 (2010).

#157687 - $15.00 USD Received 21 Nov 2011; revised 17 Jan 2012; accepted 18 Jan 2012; published 1 Feb 2012
(C) 2012 OSA

31. S. Kumar, "Development of terahertz quantum-cascade lasers," Massachusetts Institute of Technology 163–166 (2007).
32. C. W. I. Chan, S. Fathololoumi, E. Dupont, Z. R. Wasilewski, S. R. Laframboise, D. Ban, Q. Hu, and H. C. Liu, "A terahertz quantum cascade laser operating up to 193 K," Presented at 11th International Conference on Intersubband Transitions in Quantum Wells, Badesi, Italy (2011).
33. The waveguide loss of 22.1 cm^{-1} was calculated for the Au-Au device without the top n^+ layer ($\sim$ 170 μm wide and 1.98 mm long). The estimated cavity loss is, therefore, reduced for $\sim$ 3 cm^{-1} (1.9 cm^{-1} from the waveguide loss and 1.1 cm^{-1} from the mirror loss), as compared to the estimated cavity loss of the Au-Au device with the top n^+ layer ($\sim$ 144 μm wide and 1 mm long), lasing up to 180 K. The MC simulations at 12.8 kV/cm and 3.22 THz showed a gain reduction of $\sim$ 4 cm^{-1}.
34. J. Faist, F. Capasso, A. L. Hutchinson, L. Pfeiffer, and K. W. West, "Suppression of optical absorption by electric-field-induced quantum interference in coupled potential wells," Phys. Rev. Lett. **71,** 3573–3576 (1993).
35. L. A. Dunbar, R. Houdré, G. Scalari, L. Sirigu, M. Giovannini, and J. Faist, "Small optical volume terahertz emitting microdisk quantum cascade lasers," Appl. Phys. Lett. **90,** 141114 (2007).
36. C. Weber, A. Wacker, and A. Knorr, "Density-matrix theory of the optical dynamics and transport in quantum cascade structures: the role of coherence," Phys. Rev. B **79,** 165322 (2007).
37. A. Mátyás, P. Lugli, and C. Jirauschek, "Photon-induced carrier transport in high efficiency midinfrared quantum cascade lasers," J. Appl. Phys. **110,** 013108 (2011).
38. A. Mátyás, T. Kubis, P. Lugli, and C. Jirauschek, "Comparison between semiclassical and full quantum transport analysis of THz quantum cascade lasers," Physica E **42,** 2628 (2010).

1. Introduction

Nearly a decade after the first demonstration of terahertz quantum cascade lasers (THz QCL) [1], the quest for room temperature operation continues, through designing new lasing schemes with higher gain [2–10], and lowering the waveguide loss [11–13]. So far among all existing designs, the three-well resonant phonon based THz QCLs, originally proposed by Luo et *al*. [3], have demonstrated the best temperature performance [5,14]. Several theoretical models have been employed to understand the details of charge transport and optical gain within THz QCLs, based on various approaches such as density matrix (DM) [15–17], non-equilibrium Green function [18, 19], and Monte Carlo (MC) techniques [20–22]. With a simplified DM model it has been found that the population inversion ($\Delta\rho$) of three well resonant phonon based active regions is lowered by parasitic injection and extraction tunneling channels [16,17]. Kumar et *al*. proposed to make the lasing transition more diagonal in order to increase the upper lasing state lifetime and reduce the strength of undesired tunneling couplings, which leads to an improved population inversion at high temperatures. This strategy brought the maximum operating temperature T_{max} to 186 K at 3.9 THz [5]. However, the gain of THz QCL depends on the product of population inversion and oscillator strength f ($g_{isb} \propto f.\Delta\rho$), and hence low oscillator strength is expected to reduce the gain. The temperature dependence of population inversion, spectral bandwidth and gain for several degrees of diagonality and laser frequencies has been studied in Ref. [23], through a MC approach. For frequencies above $\sim$ 3.5 THz, it was found that the diagonality of the lasing transition is beneficial between 150-200 K. Below $\sim$ 3.5 THz, the diagonality marginally improves population inversion at high temperatures and hence does not compensate for lowering of the oscillator strength.

This work reports experimental results on optimizing the diagonality of THz QCLs designed at $\sim$3.6 THz, and presents a device that lases up to 199.5 K, by increasing the oscillator strength to 0.58. Even though the optimization process was assisted by the DM model, which considers transport and gain as coherent processes with dephasing mechanisms, the voltage dependence of the laser frequency could be better described by a semi-classical MC approach. This paper is organized as follows. In the next section we describe the optimization process and the design with the best temperature performance. In Section 3 experimental results of the optimized design with T_{max} of 199.5 K are presented. In Section 4 the electric field dependence of the laser spectra is discussed using a simple oscillator strength model and is further illustrated by MC simulations. We summarize our results in the last section.

#157687 - $15.00 USD Received 21 Nov 2011; revised 17 Jan 2012; accepted 18 Jan 2012; published 1 Feb 2012
(C) 2012 OSA

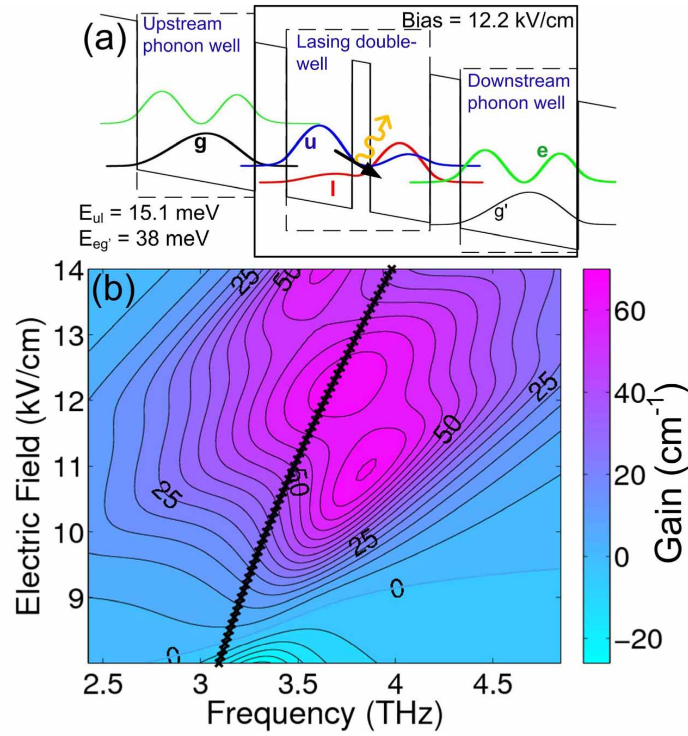

Fig. 1. a) Conduction band diagram of the designed THz QCL with $f_{ul} = 0.475$, in isolated-well picture at 12.2 kV/cm, b) Contour plot of gain spectra (unit of cm^{-1}) for different electric fields at a lattice temperature of 10 K. The line with crosses represents the energy difference between upper (g) and lower (l) lasing states as a function of electric field. Doping level is 3×10^{10} cm^{-2}.

2. Optimization of THz QCL by a density matrix model

The design process started by finding the lasing double wells with intersubband resonance at 15 meV, using $GaAs/Al_{0.15}Ga_{0.85}As$ material system. Five different oscillator strengths within the lasing double-well, $f_{ul} \approx 0.25, 0.30, 0.35, 0.41$ and 0.47 at a design electric field of around 12 kV/cm, were selected [24]. Initially we assumed the lasing double-well (with l: the lower and u: the upper lasing states) is isolated from the upstream and downstream phonon wells. Each of the two phonon wells, shown in Fig. 1a, contains one injector (g) and one extractor (e) state. The injection and extraction barrier thicknesses play important roles in populating and depopulating the lasing levels [25, 26], as well as in defining the linewidth and amplitude of the gain [17]. The optimization of the barrier thicknesses for each oscillator strength were performed using a simplified DM approach [17]. Despite its rather simple and fast computation process, the DM model provides essential design guidelines that include all the tunneling cou-

#157687 - $15.00 USD Received 21 Nov 2011; revised 17 Jan 2012; accepted 18 Jan 2012; published 1 Feb 2012
(C) 2012 OSA

plings and several scattering mechanisms. The tunneling coupling strengths between the four states are calculated using a tight-binding approach. The temperature, at which the gain coefficient of $g_{isb} \simeq 35\ cm^{-1}$ was maintained, was targeted to be maximized, without constraining the threshold current density. For each of the designs, several phonon well thicknesses were considered during the optimization process. This exercise converged towards rather thin injection and extraction barriers, and we found the pairs of states across these barriers (*g*-*u* for injection and *l*-*e* for extraction) are aligned at about the same electric field. The convergence of the model towards thinner barriers is mostly driven by the maximization of population inversion, but is constrained by the gain broadening that is induced by the tunneling couplings and the parasitic leakages (the wrong injection: $g \rightarrow l$ and the wrong extraction: $u \rightarrow e$ channels).

Figure 1a depicts the isolated-well picture of the design with $f_{ul} = 0.475$, the lasing double-well being isolated from upstream (injection) and downstream (extraction) phonon wells (this structure will be discussed for the rest of the paper). In this picture, at the design electric field of 12.2 kV/cm, the energy difference between the lasing states reads $E_{ul} = 15.1$ meV, with the injector and extraction coupling of $h\Omega_{gu} = 1.38$ meV and $h\Omega_{le} = 2.47$ meV, respectively. The upper lasing state lifetime, set by LO phonon emission, is $\tau_{ul} = 0.45$ ps at kinetic energy $E_{LO} - E_{ul}$. Figure 1b shows the DM calculation results of the gain spectra of the same design at different electric fields for a lattice temperature of 10 K [27]. The DM model predicts that the energy position of the gain peak is slightly higher than the energy difference between the upper and lower lasing states (E_{ul}), below the design electric field. Figure 1b shows three separate peaks in the simulated contour plot, as opposed to a single peak gain in the structure discussed in the Ref. [17]. This is believed to be due to the large coupling strength for the designed structure in the present work, which results in large frequency shift of the doublet transitions with respect of the bare transition $E_u \rightarrow E_l$ (see Fig. 8 of Ref. [17]).

The DM calculations did not convincingly reveal an optimum point for the oscillator strength, similar to MC optimization results in Ref. [23]. With this DM model, it has been found that, with optimized barrier thicknesses and a threshold gain of 30 cm^{-1}, T_{max} of ~ 170 K could be achieved for all the designs [28]; hence it is necessary to search for the optimum point experimentally. The five designs were grown separately on semi-insulating GaAs substrates by molecular beam epitaxy with a 10 μm thick active region and a sheet electron density of $3 \times 10^{10}\ cm^{-2}$ per period using a 3D Si-doping within the middle 5 nm of the phonon well. The active region was sandwiched between 100 nm of $5 \times 10^{18}\ cm^{-3}$ bottom n^+ GaAs and a top stack of 50 nm of $5 \times 10^{18}\ cm^{-3}$ and 10 nm of low temperature grown $5 \times 10^{19}\ cm^{-3}$ n^+ GaAs layers. Special emphasis was put on minimizing the drift of fluxes for Ga and Al during this long growth process. The X-ray diffraction rocking curve could be perfectly fitted with nominal parameters, with no extra broadening of satellites peaks, confirming the excellent stability of the growth rates (better than 0.5%) throughout the active region. The wafers were then processed into THz QCL structures with Au double metal waveguides. All devices have the following dimensions: $\sim 144\ \mu$m wide ridges with $\sim 130\ \mu$m wide top Ti/Au metallization forming a Schottky contact, and ~ 1 mm long Fabry-Perot resonator. An In-Au wafer bonding technique was used [11, 13] and the ridges were fabricated by reactive-ion etching. All five devices lased above 160 K, with the highest T_{max} of 180 K observed from the device with $f_{ul} = 0.475$. A module of this design consists of three wells and three barriers with the layer thicknesses of **43**/89/**24.6**/81.5/**41**/160 Å starting from the injector barrier - the barriers are indicated in bold font.

Figure 2 shows the conduction band diagram and the square of extended wavefunctions of the design with $f_{ul} = 0.475$, with large overlap of mixed states *1* with *2* and states *3* with *4*. This structure at 12.2 kV/cm results in a total oscillator strength between the lasing states of $f_{13} + f_{23} = 0.582$, compared to $f_{ul} = 0.475$ calculated from the isolated-well picture. At this

#157687 - $15.00 USD Received 21 Nov 2011; revised 17 Jan 2012; accepted 18 Jan 2012; published 1 Feb 2012
(C) 2012 OSA

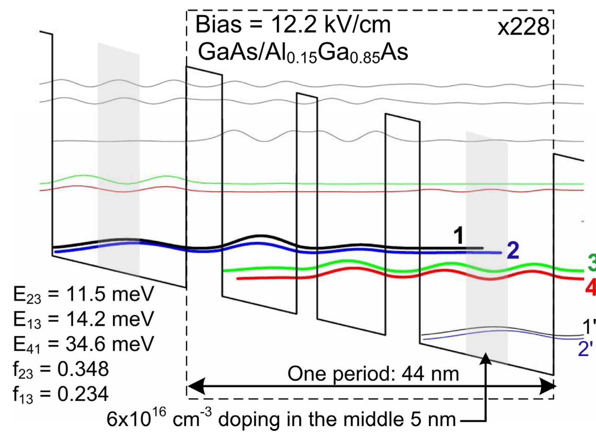

Fig. 2. Conduction band diagram and squared moduli of wavefunctions of the optimized $f_{ul} = 0.475$ THz QCL at the design electric field of 12.2 kV/cm. It consists of three wells and three barriers with the layer thicknesses of **43**/89/**24.6**/81.5/**41**/160 Å starting from injector barrier - the barriers are indicated in bold fonts.

electric field, the *1*→*4* and *2*→*4* transitions contribute marginally to the total oscillator strength. The increase of calculated oscillator strength with the extended wavefunctions as opposed to the isolated-well picture suggests non-negligible electron-light coupling between the upper lasing state, *u*, and the extraction state, *e*. Since there is a large population inversion between these two states, the transition *u*→*e* is expected to contribute positively to the gain. This particular DM model uses a basis of states from isolated lasing and phonon wells, meaning that the states *u* and *e* belong to two different Hamiltonians and are not orthogonal to each other. Therefore, in its present form, this DM model fails to accommodate dipole moments other than z_{ul}, and further work is required to include interwell electron-light scattering.

The design with $f_{ul} = 0.475$ has very similar double and phonon wells, as the device reported by Belkin et *al*. in Ref. [14]: **51**/90/**24**/81/**46**/163 Å, which lased up to 174 K. The two structures mainly differ by thicker injection/extraction barriers in Belkin's design that lead to smaller injection ($h\Omega_{inj} = 0.91$ meV) and extraction ($h\Omega_{ext} = 1.89$ meV) couplings. For Belkin's structure, the states *g* and *u* are aligned at 11.8 kV/cm on the injection side, and the states *l* and *e* are aligned at 11.1 kV/cm on the extraction side. At the field of maximum gain, states *1* and *2* are perfectly mixed, whereas states *3* and *4* are localized in the double well and phonon well, respectively, reducing their overlap and hence the depopulation rate as compared to our design. Comparing the two structures using MC simulation reveals that the net scattering rate from level *3* to *4* is 6 % higher in our design. The increased injection anticrossing in our structure leads to reduced backscattering *2*→*1* and, therefore, higher net scattering from *1* to *2* by 8 %. The larger anticrossing facilitates a larger occupation of level *2* and a less occupied level *1* due to the quasi-Fermi distribution of electrons in the lowest states of the injector well. This is also confirmed by self-consistent MC simulations. Consequently in our design level *2* populates more heavily, while it has also the highest oscillator strength with level *3*, at the electric field of maximum gain. On the other hand, the anticrossing between levels *g* and *e*, around 8-9 kV/cm, is higher in our structure (0.97 meV) than that in Belkin's (0.56 meV), which should result in a higher threshold current density in our device [5,28].

#157687 - $15.00 USD Received 21 Nov 2011; revised 17 Jan 2012; accepted 18 Jan 2012; published 1 Feb 2012
(C) 2012 OSA

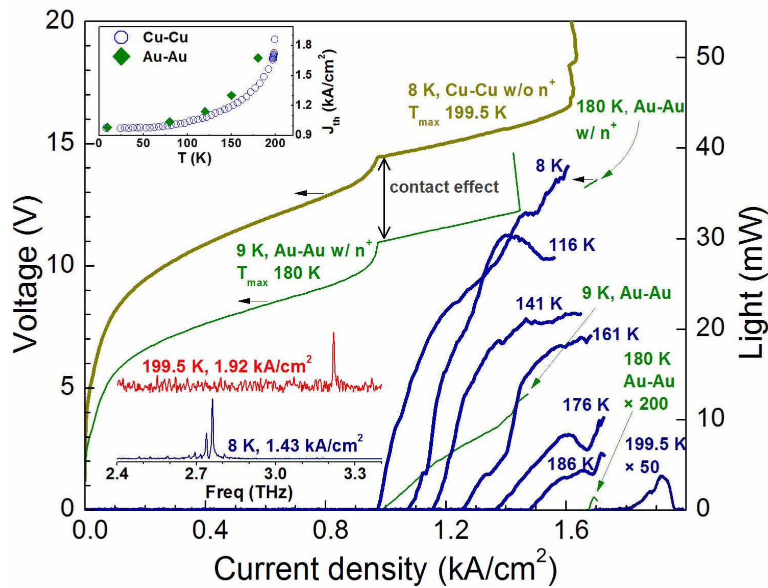

Fig. 3. Collected THz light (optical output power) versus current density at different heat sink temperatures, for the THz QCL with $f_{ul} = 0.475$. For comparison, the thicker and thinner lines are the LI curves of the Cu-Cu (lased up to 199.5 K, 170×1800 μm^2 in dimension) and Au-Au (lased up to 180 K, 144×1000 μm^2 in dimension) devices, respectively. Since the two devices are not measured in the same optical setup, the waveguide loss difference can not be estimated from the external differential efficiencies. The curves with a horizontal left arrow are the voltage-current density characteristics of the Cu-Cu based laser without (w/o) the top n$^+$ layer at 8 K and of the Au-Au-based laser with (w/) this layer at 9 K and 180 K. The insets show the spectra of the Cu-Cu based lasing device, at 8 K and 199.5 K, and the threshold current density versus temperature for two devices.

3. Experimental results

Additional improvement of the T_{max} for the optimized design requires further lowering the waveguide loss and improving heat dissipation. Hence a Cu-Cu based process with lower waveguide loss and better heat dissipation was employed. Moreover, the 100 nm thick top n$^+$ contact layer was removed for further lowering the waveguide loss, similar to the device with $T_{max} = 186$ K reported in [5]. A Cu-Cu based double metal waveguide for the THz QCLs was fabricated, using Cu-Cu wafer bonding and standard photolithography. A bottom and top metal stacks of Ta/Cu (10/600 nm) and Ta/Cu/Ti/Au (10/300/20/150 nm) were used, respectively, for the contacts. Wet etching was performed ($H_3PO_4/H_2O_2/H_2 : 3/1/25$) to etch through the entire thickness of the 10 μm thick active region. The ridge waveguide of fabricated THz QCLs is ~ 170 μm wide. The substrate of the samples was thinned down to ~ 150 μm [29] and then cleaved into laser bars with a 1.8 mm long Fabry-Perot resonator. The laser bars were then gold plated on the back side, indium soldered (epilayer side up) on a copper package and then mounted in a closed-cycle cryostat for measurements.

Figure 3 shows pulsed light-current-voltage (LIV) characteristics of the fabricated device from 8 K to 199.5 K, with a pulse duration of 300 ns and repetition rate of 300 Hz (a duty cycle of $\sim 10^{-4}$). The device showed a T_{max} of 199.5 K, while a peak output power of more than 6

#157687 - $15.00 USD Received 21 Nov 2011; revised 17 Jan 2012; accepted 18 Jan 2012; published 1 Feb 2012
(C) 2012 OSA

mW could still be collected at 186 K - the previous T_{max} record for THz QCLs. Higher duty cycle pulse would result in elevated active region temperature and hence reduces the measured T_{max} [30]. A 2D waveguide loss calculation based on the isotropic Drude model for the laser active region was performed for both Au-Au and Cu-Cu device structures at 180 K and 200 K, respectively, using COMSOL [13]. The calculations predicted a waveguide loss reduction of 4.6 cm^{-1} (from 24 to 19.4 cm^{-1}) by employing the Cu-Cu waveguide and removing the top contact n^+, and hence explains the 19 K improvement in the T_{max}. This is fairly consistent with previous observations on several four-well resonant phonon QCLs at similar frequency [31]. Similarly, the MC simulations (at 12.8 kV/cm) showed a degradation of $\sim 5.2\ cm^{-1}$ on the gain at 3.22 THz, when temperature increased from 180 K to 199.5 K; this is in good agreement with the estimated change of cavity loss ($\sim 5.6\ cm^{-1}$: 4.6 cm^{-1} from the waveguide loss and 1 cm^{-1} from the mirror loss). For a fair comparison, one cannot exclude the effect of process variation (for instance the ridge etching process) between the Au-Au device (fabricated at NRC) and Cu-Cu device (fabricated at MIT), on the improvement of T_{max}. At low temperatures (below 120 K), both waveguides show very similar threshold current densities but a discrepancy appears above 120 K (see inset of Fig. 3), suggesting that the waveguide loss increases faster with temperature for the Au-Au device. Furthermore, a Au-Au based device ($\sim 170\ \mu$m wide and 1.98 mm long) without the top n^+ layer was fabricated and a T_{max} of 195 K was recorded [32,33].

Population inversion starts slightly above the bias of resonance between the levels g and e. On the voltage-current density characteristics of the Au-Au device, with the top n^+ layer, a signature of this tunneling resonance is observed at $\sim$10 V. This agrees well with the theoretical electric field of 8.9 kV/cm for g-e resonance, if we consider 0.8 V Schottky voltage drop on the top contact [13]. The significant difference in the IV curves of the two devices (as shown in Fig. 3) is related to the absence of the top 100 nm thick n^+ layer in the Cu-Cu device. The Au-Au based laser shows a lower dynamic range in current than the Cu-Cu device, the origin of which is still unclear [31]. One hypothesis is that the driving electrical circuit might push the laser into the negative differential resistance (NDR) region before the electric field reaches its design value ($\sim$ 12.2 kV/cm, or $\sim$ 13 V in voltage when including the voltage drop across Schottky contact). As shown in Fig. 3, the Au-Au device stops lasing abruptly at 12.2 V, while its differential resistance from threshold to $J_{max} = 1450\ A/cm^2$ remains low and constant at 1.8-1.9 Ω. Following the same trend before NDR and extrapolating the voltage to 13 V, similar maximum current density ($\sim 1600\ A/cm^2$) as the Cu-Cu device is estimated. At 10 K, the threshold current density is $1\ kA/cm^2$, and increases exponentially with temperature ($T_0 = 39$ K), as depicted in the inset to Fig. 3. This T_0 value is much lower than that reported in Refs. [4,5].

4. Analysis of lasing frequency

The lower-left inset to Fig. 3 shows the spectra of the Cu-Cu lasing device at 8 K and 199.5 K. At 199.5 K, the laser showed a single mode emission at 3.22 THz, corresponding to $T_{max} \sim 1.28 h\omega/\kappa_B$. At 8 K and close to maximum power, the device lases at 2.75 THz, which is closer to the value predicted by solving the Schrödinger equation along several periods as what was done for Fig. 2. Figure 4 shows the energy spacing between all four extended energy states (*1* to *4*) and their respective oscillator strength. One can see the transitions $1 \rightarrow 3$ and $2 \rightarrow 3$ dominate over the other two around the design electric field (12.2 kV/cm). They exchange their oscillator strength around 11.8 kV/cm, $1 \rightarrow 3$ being stronger below this electric field. The other transitions, $1 \rightarrow 4$ and $2 \rightarrow 4$, are not very optically active, which can be explained by a destructive quantum interference between dipole moments [34]. This interference effect is not included in our DM model, since it only considers one dipole moment (between the two states

#157687 - $15.00 USD Received 21 Nov 2011; revised 17 Jan 2012; accepted 18 Jan 2012; published 1 Feb 2012
(C) 2012 OSA

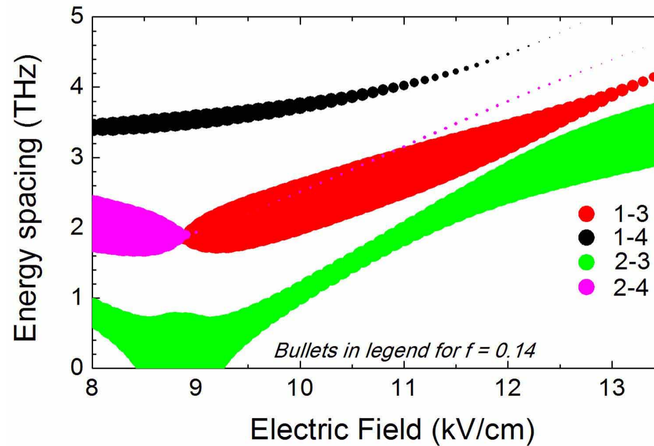

Fig. 4. Energy spacing between various extended wavefunctions in the designed THz QCL. The width of each curve at each point represents the corresponding oscillator strengths.

of the double well, z_{ul}). Below the design electric field, the gain peak frequency predicted by the DM model (Fig. 1b) is overestimated compared to the measured lasing frequency, as the *1→4* transition is the strongest transition in the DM picture (see Fig. 8a in Ref. [17]). Instead, the measured laser frequency is closer to the energy of *1→3* transition, which has the highest oscillator strength below 11.8 kV/cm. From data taken from the Au-Au device, with the top n^+ contact layer, one knows the lasing threshold occurs at ∼ 11 V, which corresponds to an electric field of 10.2 kV/cm after subtracting the extra 0.8 V due to the top Schottky contact [13]. At this field, we read from Fig. 4 $E_{13} \equiv 2.4$ THz, a value close to the observed laser frequency, 2.7 THz.

At high temperatures, lasing occurs at high electric fields; for instance at 180 K the peak power occurs at 13.45 V (Fig. 3), corresponding to an electric field of ∼12.7 kV/cm by assuming the same 0.8 V Schottky barrier. At this electric field, both the *1→3* and *2→3* transitions contribute to the gain. The peak gain frequency is, therefore, increased. At 199.5 K, the measured frequency (3.22 THz) is between the computed energy spacings at 12.7 kV/cm: $E_{13} \equiv 3.71$ THz and $E_{23} \equiv 3.02$ THz, the latter transition being more intense according to the oscillator strength picture. Considering the uncertainty in electric field due to the Schottky contact, the laser frequency at high temperature agrees well with E_{23}. This exercise of oscillator strength calculation between levels *1* to *4* indicates that the MC approach, which uses the extended states and considers all the broadening and population inversion between levels *1* to *4*, is probably better suited to predict the laser frequency than the present simplified DM model. Therefore to predict the laser frequency at different temperatures and biases, an MC based approach is employed.

Figure 5a to 5f depicts the measured spectra of the Au-Au device, with the top n^+ layer, at different biases and temperatures. For all temperatures, the spectra show a consistent blue (Stark) shift at higher biases. The highest lasing frequency is measured close to the T_{max}, as at this temperature no NDR is observed and hence high biases are achievable. The device with the top n^+ layer provides us with rather accurate voltage measurement and hence the voltage across the active region can be estimated by considering the 0.8 V Schottky voltage drop across

#157687 - $15.00 USD Received 21 Nov 2011; revised 17 Jan 2012; accepted 18 Jan 2012; published 1 Feb 2012
(C) 2012 OSA

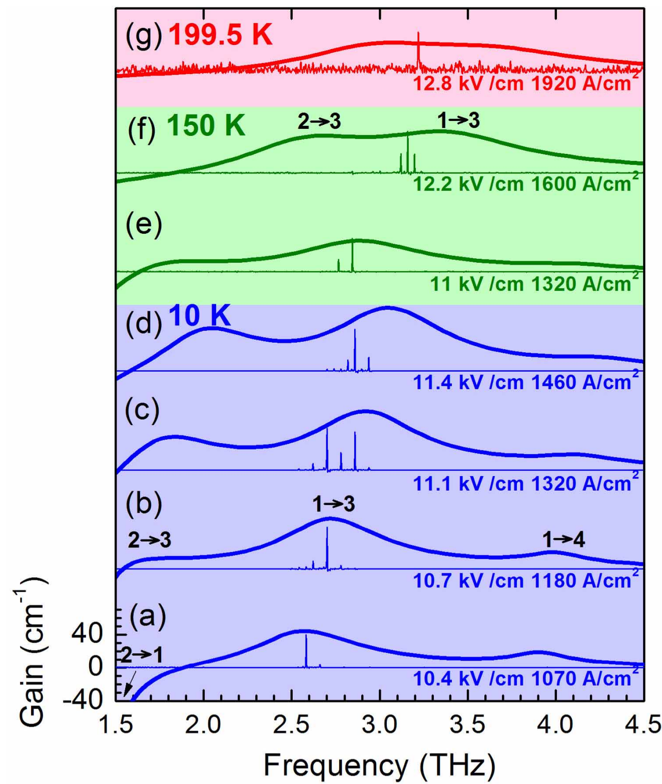

Fig. 5. Spectra of the lasing device at various current densities at 10 K (a to d), 150 K (e and f), and 199.5 K (g), along with the comparison with the calculated gain spectra using MC simulation. The corresponding measured current density along with the simulated bias values are indicated within each plot, assuming 0.8 V Schottky voltage drop across the top contact. Plots (a) to (f) show the laser spectra for the Au-Au device with the top n^+ GaAs contact layer ($T_{max} = 180$ K); plot (g) shows the laser spectra for the Cu-Cu device ($T_{max} = 199.5$ K). The vertical scales for all plots are the same.

the top contact [13]. The gain spectra of the device at different biases and temperatures were recalculated using the MC approach [22], the results of which are compared with the measured spectra in Fig. 5. The MC simulation used 100 Å for the correlation length and 1.2 Å for the mean height, in modeling the interface roughness. The mean height used in this work is relatively low, reflecting the high growth quality of these wafers [22]. Figure 5 shows a good agreement between the measured spectra and the peak of the gain calculated using MC simulation. At 199.5 K (Fig. 5g, the Cu-Cu device), the simulated gain is flat in the 3-3.5 THz range, due to closely spaced *1→3* and *2→3* transitions. Therefore, the frequency position of the peak gain becomes very sensitive to the electric field, which along with the waveguide loss frequency dependence sets the lasing frequency at 3.22 THz. At T_{max}, the MC model predicts a peak–gain or equivalently a waveguide loss of 37.5 cm^{-1}, a value that is consistent with a previous measurement by cavity frequency pulling [35]. Since the employed MC model does

#157687 - $15.00 USD Received 21 Nov 2011; revised 17 Jan 2012; accepted 18 Jan 2012; published 1 Feb 2012
(C) 2012 OSA

not include stimulated emission, the simulated current and experimental laser IV should be compared only when transport is dominated by the non-radiative scattering, i.e. only for high temperatures [37]. From 180 K and above, the peak current simulated by MC is about 10-15% smaller than experimental values. This small discrepancy could originate from the uncertainty in interface roughness and leakage channels through high energy states that are not included in the calculations.

By nature, the two models used in this paper are very different. The DM model takes into account gain and transport coherence, but requires phenomenological input parameters. The present implementation of DM should be treated with caution, as it considers only intrawell scatterings and hence only one (intrawell) dipole moment. This shortcoming is not inherent to DM but related to the choice of basis of the states, which has not been addressed yet. The MC approach, on the other hand, is based on the Boltzmann equation and uncorrelated inter- and intra-subband hopping events. It considers all known scattering processes, including e-e scattering. Similarly, MC simulations should also be treated with caution, particularly for the states with small anticrossing (e.g. thick barriers), as it does not consider wavefunction localization in the presence of dephasing [20,21]. Though recognizing these important differences, this work did not attempt to validate one model against the other. However, one has to address the importance of coherent effects in THz QCLs, a topic which is highly debated [36,38] and may be crucial for further improvement of the THz QCLs.

5. Conclusion

With a density matrix approach we have optimized the diagonality of three-well resonant-phonon based THz QCLs in order to maximize the gain at high temperatures. This yielded the design, growth and fabrication of several structures with rather thin tunneling barriers and with almost perfect level alignment on both injection and extraction sides. In the optimized structure, the population inversion was maximized at high temperatures but at the expense of having higher current densities. From 0.25 to 0.47 diagonality, all wafers processed as standard 1-mm long Au double–metal waveguide showed maximum operating temperature above 160 K; the best structure in term of temperature performance ($T_{max} = 180$ K) had a total 0.58 oscillator strength. To further increase the T_{max}, the waveguide loss was reduced by employing a Cu-Cu structure and removing the top n^{+} contact layer; T_{max} of 199.5 K was recorded for a 3.22-THz lasing frequency. Even though the simplified density matrix model was the key tool, providing guidelines for the gain optimization, it was not well adapted to explain the laser frequency, because only one dipole moment was included in the model, restriction related to the choice of the basis. Consequently, to illustrate the voltage dependence of laser frequency, we used a semiclassical Monte Carlo approach.

Acknowledgment

The authors would like to acknowledge support from Natural Science and Engineering Research Council (NSERC) of Canada, from Canadian Foundation of Innovation (CFI) and from the Ontario Research Fund (ORF). HCL thanks funding by the National Major Basic Research Program (2011CB925603) and the Shanghai Municipal Major Basic Research Program (09DJ1400102). The work at MIT is supported by NASA and NSF.

#157687 - $15.00 USD Received 21 Nov 2011; revised 17 Jan 2012; accepted 18 Jan 2012; published 1 Feb 2012
(C) 2012 OSA